Journal of Physics: Conference Series **160** (2009) 012017 doi:10.1088/1742-6596/160/1/012017

# Crystal Calorimeters in the Next Decade

**Ren-yuan Zhu**

California Institute of Technology, Pasadena, CA 91125, USA

E-mail: zhu@hep.caltech.edu

**Abstract.** Crystal calorimeter has traditionally played an important role in precision measurement of electrons and photons in high energy physics experiment. Recent interest in calorimeter technology extends its application to measurement of hadrons and jets with dual readout. Potential application of new generation scintillating crystals of high density and high light yield, such as LYSO, in high energy physics experiment is described. Candidate crystals for the proposed homogeneous hadronic calorimeter concept is also discussed.

## 1. Introduction

Total absorption shower counters made of inorganic crystal scintillators have been known for decades for their superb energy resolution and detection efficiency [1]. In high energy and nuclear physics, crystal calorimeters have been constructed, and their use has been a key factor in the successful physics programs of many experiments. The use of crystals for electromagnetic calorimeter in high energy and nuclear physics experiment is well understood. With proper calibration and monitoring, crystal calorimeters achieve their designed resolution for photon and electron measurement [2]. Recent interest in homogeneous crystal hadronic calorimeter extends its application to measurement of hadrons and jets with high resolution [3]. This concept adapts dual readout for both Cherenkov and scintillation light, which is extensively studied recently by the Dream collaboration [4]. Section 2 of this paper describes optical and scintillation properties of heavy crystal scintillators commonly used in particle physics experiment. Fast and bright crystals discovered in the last two decades, such as cerium doped lutetium oxyorthosilicate ($Lu_2(SiO_4)O$ or LSO) [5], cerium doped lutetium yttrium oxyorthosilicate ($Lu_{2(1-x)}Y_{2x}SiO_5$, LYSO) [6] and cerium doped lanthanum tri-halides,e.g. $LaCl_3$ and $LaBr_3$[7] are also covered. The expected performance of a LYSO electromagnetic calorimeter is elaborated in Section 3. Section 4 discusses candidate crystals for the homogeneous crystal hadronic calorimeter concept.

## 2. Properties of Crystal Scintillators

Table 1 lists basic properties of heavy crystal scintillators: NaI(Tl), CsI(Tl), $BaF_2$, $CeF_3$, bismuth gemanade ($Bi_4Ge_3O_{12}$ or BGO), lead tungstate ($PbWO_4$ or PWO) and LSO [8]. All, except $CeF_3$, have either been used in, or actively pursued for, high energy and nuclear physics experiments. LSO and LYSO crystals are widely used in the medical industry. Mass production capabilities exist for all these crystals.

Figure 1 is a photo showing twelve crystal samples. In addition to samples listed in Table 1 pure CsI, CsI(Na), LYSO as well as $LaCl_3$ and $LaBr_3$ are also shown in this photo although the last two are not yet in mass production stage. Samples are arranged in an order of their

 

**Table 1.** Properties of Heavy Crystal Scintillators with Mass Production Capability

| Crystal | NaI(Tl) | CsI(Tl) | $BaF_2$ | $CeF_3$ | BGO | $PbWO_4$ | LSO(Ce) |
|---|---|---|---|---|---|---|---|
| Density ($g/cm^3$) | 3.67 | 4.51 | 4.89 | 6.16 | 7.13 | 8.3 | 7.40 |
| Melting Point (°C) | 651 | 621 | 1280 | 1460 | 1050 | 1123 | 2050 |
| Radiation Length (cm) | 2.59 | 1.86 | 2.03 | 1.70 | 1.12 | 0.89 | 1.14 |
| Molière Radius (cm) | 4.13 | 3.57 | 3.10 | 2.41 | 2.23 | 2.00 | 2.07 |
| Interaction Length (cm) | 42.9 | 39.3 | 30.7 | 23.2 | 22.7 | 20.7 | 20.9 |
| Refractive Index[a] | 1.85 | 1.79 | 1.50 | 1.62 | 2.15 | 2.20 | 1.82 |
| Hygroscopicity | Yes | Slight | No | No | No | No | No |
| Luminescence[b] (nm) | 410 | 560 | 300 | 340 | 480 | 425 | 420 |
| (at Peak) | | | 220 | 300 | | 420 | |
| Decay Time[b] (ns) | 245 | 1220 | 650 | 30 | 300 | 30 | 40 |
| | | | 0.9 | | | 10 | |
| Light Yield[b,c] | 100 | 165 | 36 | 7.3 | 21 | 0.30 | 85 |
| | | | 4.1 | | | 0.077 | |
| d(LY)/dT[b,d] (%/°C) | -0.2 | 0.4 | -1.9 | ∼0 | -0.9 | -2.5 | -0.2 |
| | | | 0.1 | | | | |
| Experiment | Crystal Ball | CLEO *BaBar* BELLE BES III | TAPS | - | L3 BELLE | CMS ALICE PrimEx Panda | SuperB |

a At the wavelength of the emission maximum.
b Top line: slow component, bottom line: fast component.
c Relative light yield of samples of 1.5 $X_0$ and with the PMT quantum efficiency taken out.
d At room temperature.

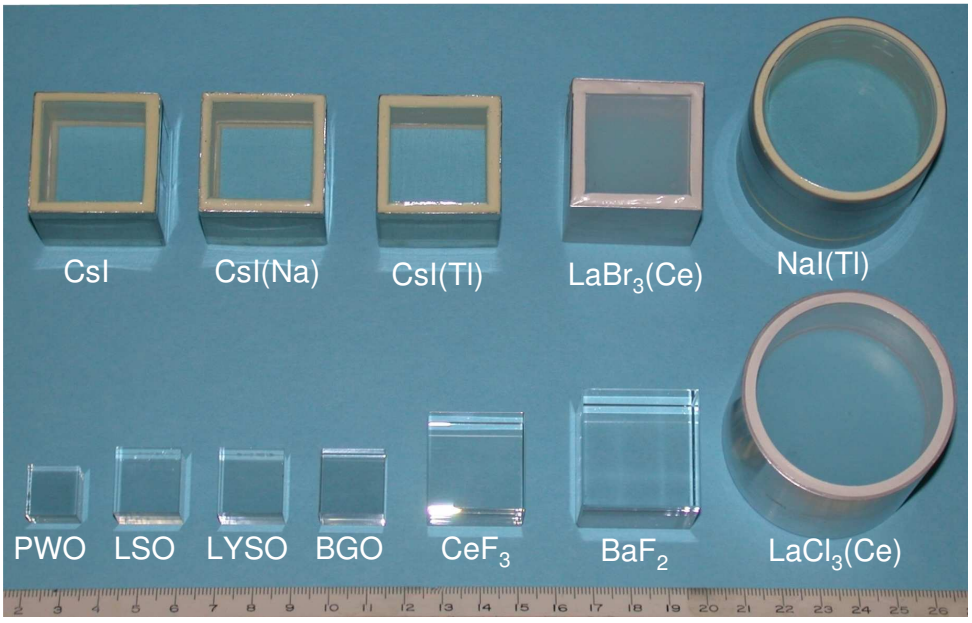


**Figure 1.** A photo shows twelve crystal scintillators with dimension of 1.5 $X_0$.

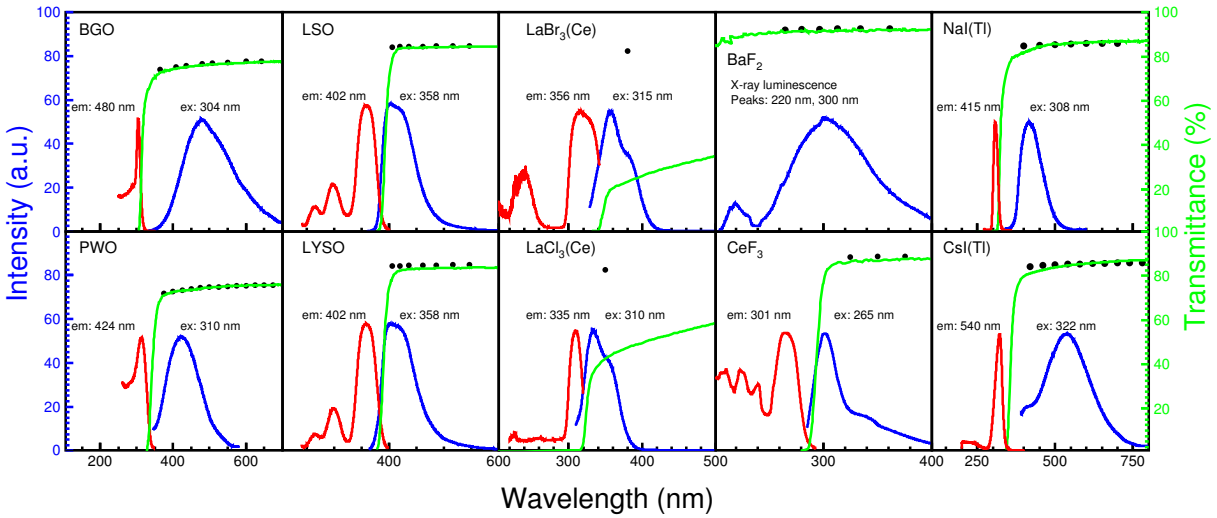


**Figure 2.** The excitation (red) and emission (blue) spectra (left scale) and the transmittance (green) spectra (right scale) are shown as a function of wavelength for ten crystal scintillators. The solid black dots are the theoretical limit of the transmittance.

density, or radiation length. All non-hygroscopic samples are wrapped with white Tyvek paper as reflector. Hygroscopic NaI, CsI, $LaBr_3$ and $LaCl_3$ are sealed in package with two ends made of quartz windows of 3 or 5 mm thick to avoid surface degradation. To minimize uncertainties in light output measurement caused by the sample size dependence all samples have a cubic shape of $1.5 \times 1.5 \times 1.5$ $X_0^3$, except NaI(Tl) and $LaCl_3$ which are a cylinder with a length of 1.5 $X_0$ and areas at two ends equaling to $1.5 \times 1.5$ $X_0^2$ to match the 2 inch diameter of the PMT cathode.

Figure 2 shows a comparison of the transmittance, emission and excitation spectra as a function of wavelength for ten samples. The solid black dots in these plots are the theoretical limit of the transmittance, which was calculated by using corresponding refractive index as a function of wavelength taking into account multiple bounces between the two parallel end surfaces and assuming no internal absorption [9]. Most samples, except $LaBr_3$ and $LaCl_3$, have

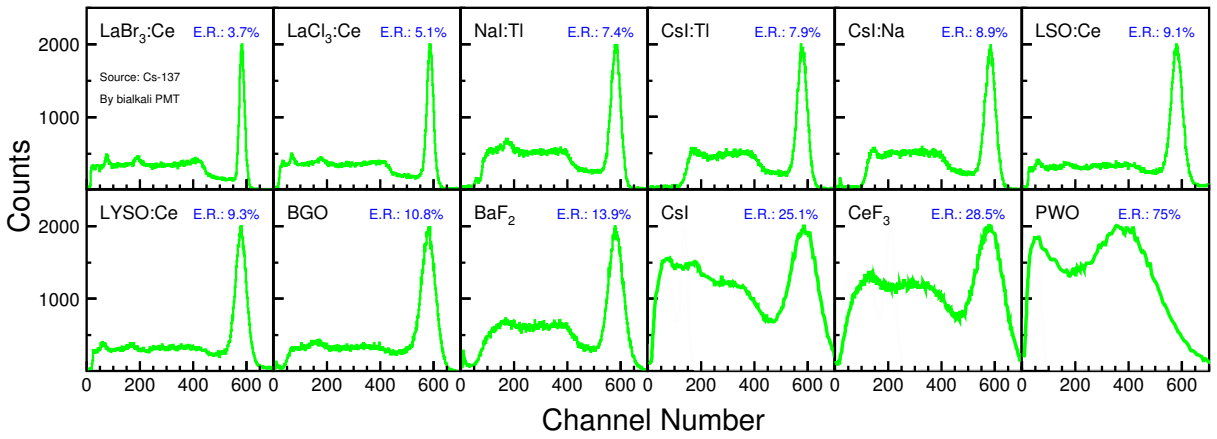


**Figure 3.** $^{137}$Cs $\gamma$-ray pulse hight spectra measured by a Hamamatsu R1306 PMT are shown for twelve crystal samples. The numerical values of the FWHM resolution (E.R.) are also shown in the figure.

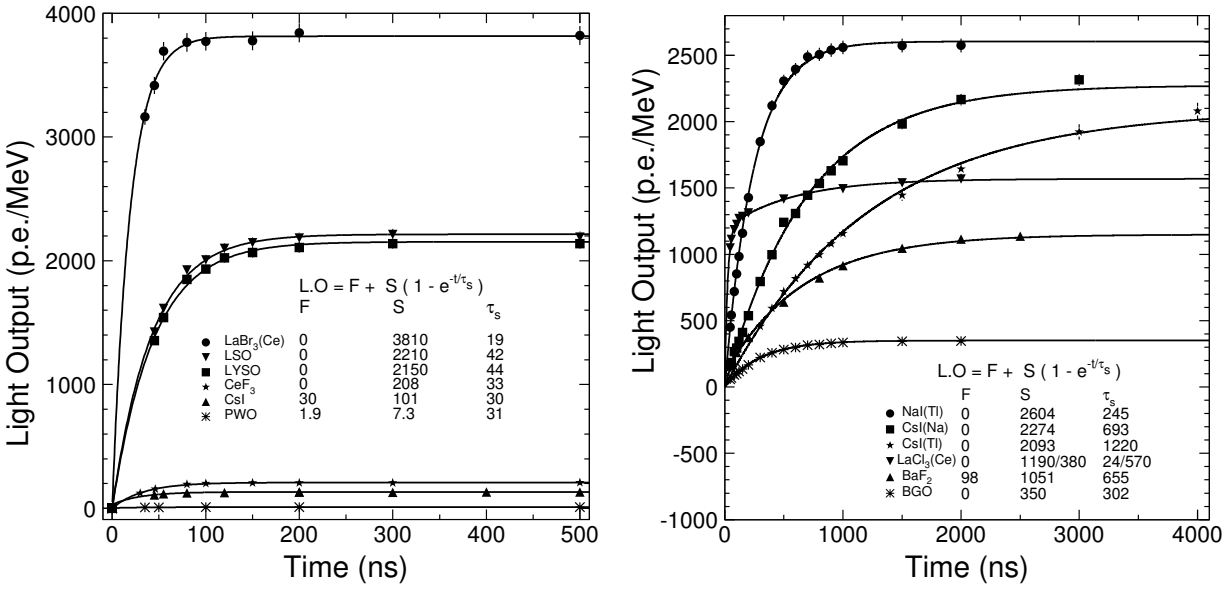


**Figure 4.** Light output measured by using a XP2254b PMT is shown as a function of integration time for six fast (Left) and six slow (Right) crystal scintillators.

their transmittance approaching the theoretical limits, indicating negligible internal absorption. The poor transmittance measured for $LaBr_3$ and $LaCl_3$ samples is probably due to scattering centers inside these samples.

It is interesting to note that $BaF_2$, BGO, NaI(Tl), CsI(Tl) and $PbWO_4$ have their emission spectra well within the transparent region showing no obvious self-absorption effect. The UV absorption edge in the transmittance spectra of LSO, LYSO, $CeF_3$, $LaBr_3$ and $LaCl_3$, however, cuts into the emission spectra and thus affects crystal's light output. This self-absorption effect is more seriously in long crystal samples used in high energy and nuclear physics experiment as extensively discussed for LSO and LYSO crystals [10].

Figure 3 shows the $^{137}$Cs $\gamma$-ray pulse hight spectra measured by a Hamamatsu R1306 PMT with bi-alkali cathode for twelve crystal samples. Also shown in these figures are the corresponding FWHM energy resolution (E.R.). $\gamma$-rays spectroscopy with a few percents resolution is required to identify isotopes for the homeland security application. It is clear that only $LaBr_3$ approaches this requirement. All other crystals do not provide sufficient energy resolution at low energies.

Figure 4 shows light output in photo-electrons per MeV energy deposition as a function of the integration time, measured by using a Photonis XP2254b PMT with multi-alkali photo cathode,

**Table 2.** Emission Weighted Quantum Efficiencies (%)

| Emission | LSO/LYSO | BGO | CsI(Tl) |
|---|---|---|---|
| Hamamatsu R1306 PMT | 12.9±0.6 | 8.0±0.4 | 5.0±0.3 |
| Hamamatsu R2059 PMT | 13.6±0.7 | 8.0±0.4 | 5.0±0.3 |
| Photonis XP2254b | 7.2±0.4 | 4.7±0.2 | 3.5±0.2 |
| Hamamatsu S2744 PD | 59±4 | 75±4 | 80±4 |
| Hamamatsu S8664 APD | 75±4 | 82±4 | 84±4 |

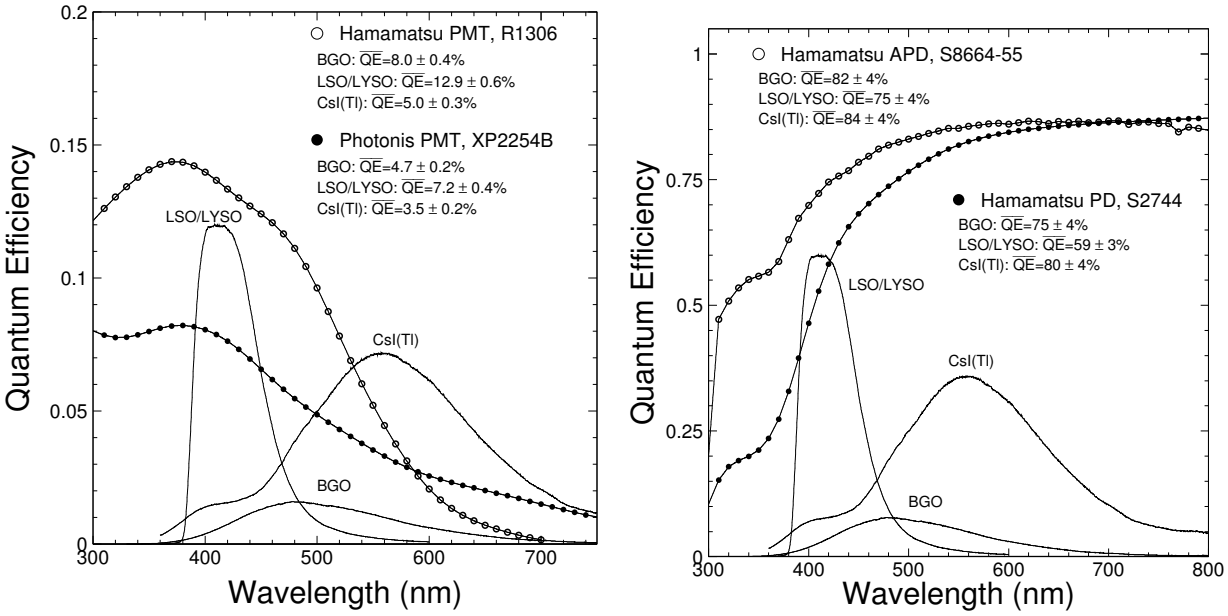


**Figure 5.** Left: Quantum efficiencies of a Hamamatsu 1306 PMT with bi-alkali cathode (open circles) and a Photonis 2254B PMT with multi-alkali cathode (solid dots) are shown as a function of wavelength together with the emission spectra of the LSO/LYSO, BGO and CsI(Tl) samples, where the area under the emission curves is proportional to their corresponding absolute light output. Right: The same for a Hamamatsu S8664 Si APD (open circles) and a Hamamatsu S2744 Si PIN diode (solid dots).

for six fast crystal scintillators (Left): $LaBr_3$, LSO, LYSO, $CeF_3$, undoped CsI and $PbWO_4$ and six slow crystal scintillators (Right): NaI(Tl), CsI(Na), CsI(Tl), $LaCl_3$, $BaF_2$ and BGO. The corresponding fits to the exponentials and their numerical results are also shown in these figures. The undoped CsI, $PbWO_4$, $LaCl_3$ and $BaF_2$ crystals are observed to have two decay components. Despite its poor transmittance the cerium doped $LaBr_3$ is noticed by its bright fast scintillation, leading to the excellent energy resolution for the $\gamma$-ray spectroscopic applications.

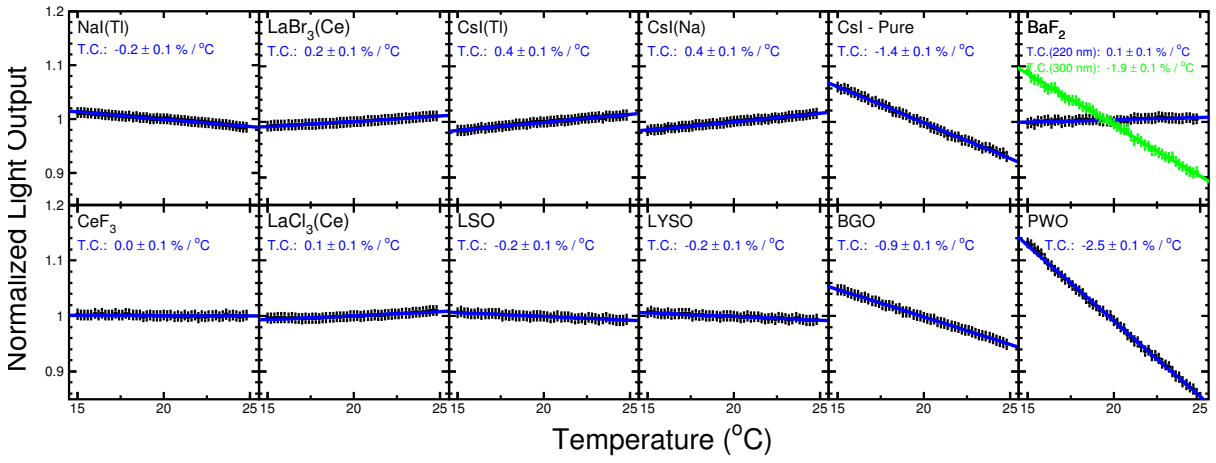


**Figure 6.** Light output temperature coefficient obtained from linear fits between 15°C and 25°C for twelve crystal scintillators.

The LSO and LYSO samples have consistent fast decay time (∼40 ns) and photo-electron yield, which is 6 and 230 times of BGO and $PbWO_4$ respectively.

Since the quantum efficiency of the PMT used for the light output measurement is a function of wavelength, it should be taken out to directly compare crystal's light output. Figure 5 shows typical quantum efficiency as a function of wavelength for a PMT with bi-alkali cathode (Hamamatsu R1306) and a PMT with multi-alkali cathode (Photonis 2254B), a Si APD (Hamamatsu S8664) and a Si PIN PD (Hamamatsu S2744). The emission spectra of LSO/LYSO, BGO and CsI(Tl) crystals are also shown in these figures. Table 2 summarized numerical result of the emission weighted average quantum efficiency for several readout devices. The light output values in Table 1 are listed with the PMT quantum efficiency taken out. The light output of LSO and LYSO crystals is a factor of 4 and 200 of that of BGO and $PbWO_4$ respectively.

Scintillation light yield from crystal scintillators may also depends on the temperature. Fig 6 shows light output variations for twelve crystal samples between 15°C and 25°C. The corresponding temperature coefficients obtained from linear fits are also listed in the figure. The numerical result of these fits is also listed in Table 1.

## 3. LYSO Crystal Electromagnetic Calorimeter

Because of their board application in medical industry large size LSO and LYSO crystals with consistent optical and scintillation properties have been routinely grown [10]. Figure 7 shows four long crystal samples of $2.5 \times 2.5 \times 20$ cm$^3$. Figure 8 shows the spectra of 0.51 MeV $\gamma$-rays from a $^{22}$Na source observed with coincidence triggers [10]. The readout devices used are a Hamamatsu R1306 PMT (Left) and 2 Hamamatsu S8664-55 APDs (Right). The FWHM resolution for the 0.51 MeV $\gamma$-ray with the PMT readout is about 12% to 13% for these long samples, which can be compared to 15% for the BGO sample. With APD readout, the $\gamma$-ray peaks are clearly visible. The energy equivalent readout noise was less than 40 keV for these long LSO and LYSO samples.

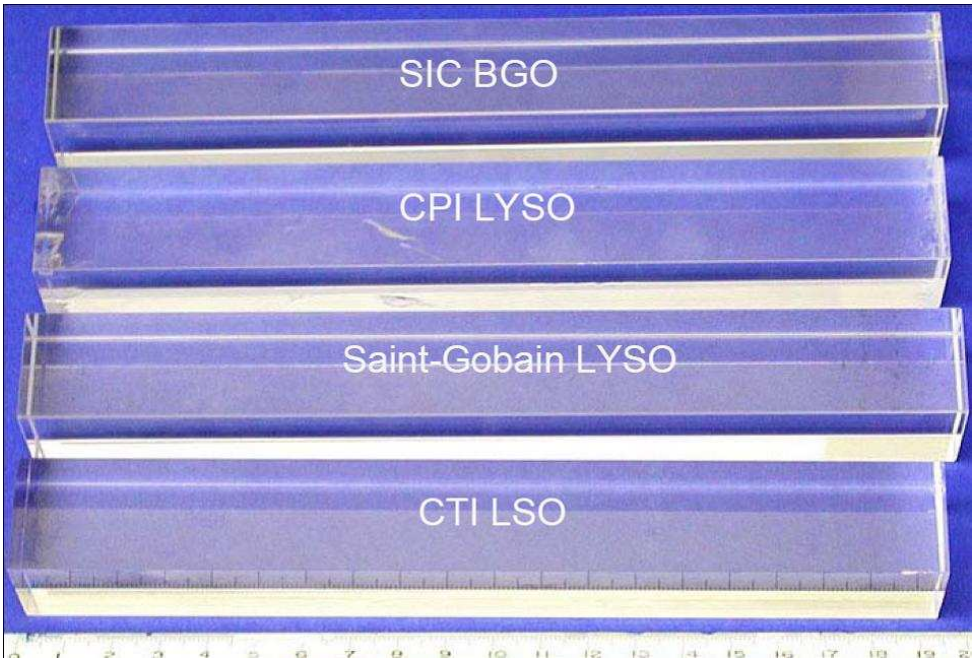


**Figure 7.** A photo shows four long crystal samples with dimension of $2.5 \times 2.5 \times 20$ cm$^3$.

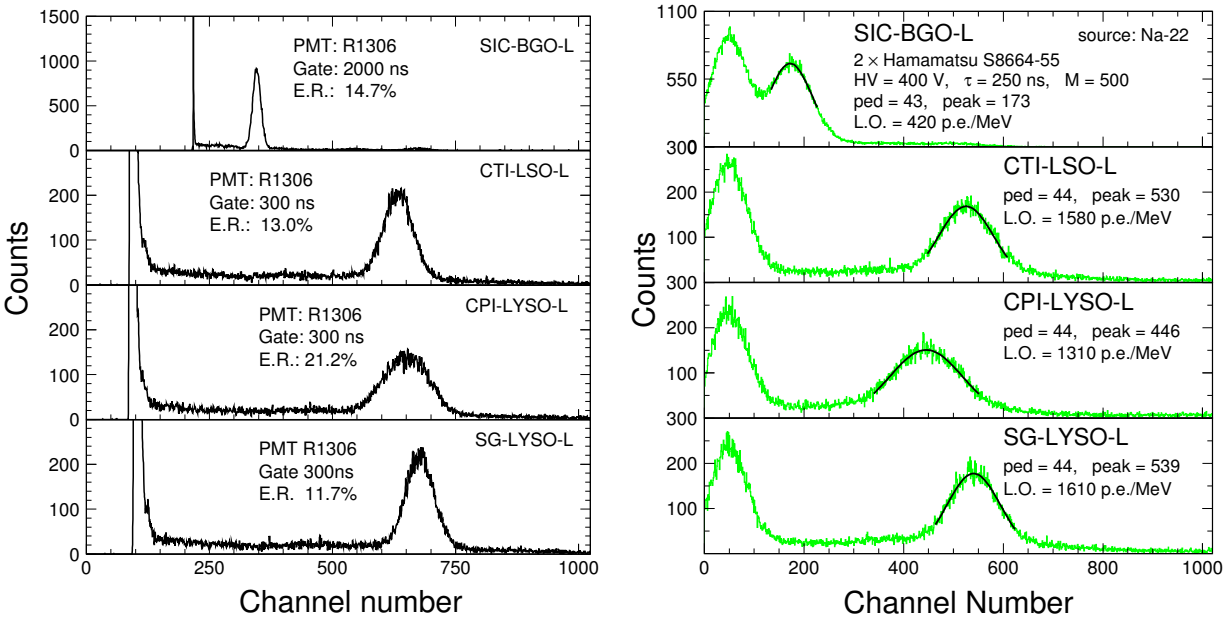


**Figure 8.** The 0.511 MeV $\gamma$-rays spectra from a $^{22}$Na source measured with a coincidence trigger using a Hamamatsu R1306 PMT (Left) and two Hamamatsu S8664-55 APDs (Right) for long BGO, LSO and LYSO samples of $2.5 \times 2.5 \times 20$ cm$^3$ size.

LSO/LYSO crystals is also found to be much more radiation hard than other crystals

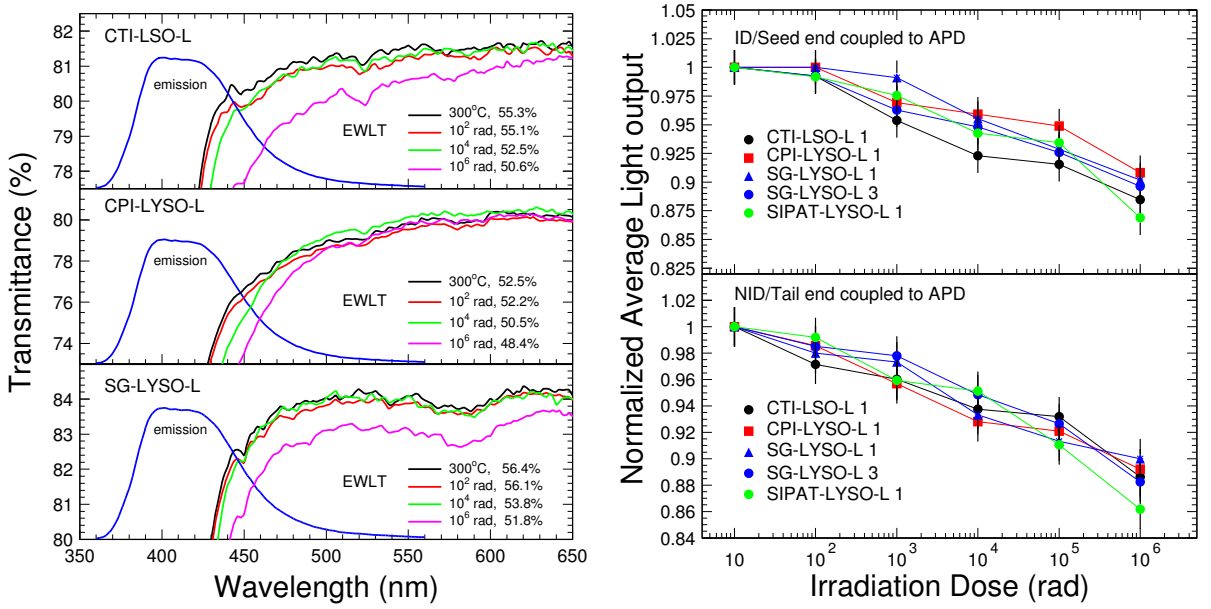


**Figure 9.** Left: Transmittance spectra are shown as a function of wavelength in an expanded scale together with the photo-luminescence spectra for three long LSO and LYSO samples before and after the irradiation with integrated doses of $10^2$, $10^4$ and $10^6$ rad. Right: Normalized light output with ID (top) and NID (bottom) end coupled to the readout device of two S8664-55 APDs is shown as a function of the integration dose for five long LSO and LYSO samples.

commonly used in high energy and nuclear physics experiment, such as BGO, CsI(Tl) and $PbWO_4$ [11]. Their scintillation mechanism is not damaged by $\gamma$-ray irradiation. Radiation damage in LSO and LYSO crystals recovers very slow under room temperature but can be completely cured by thermal annealing at 300°C for ten hours. The $\gamma$-ray induced readout noise was estimated to be about 0.2 MeV and 1 MeV equivalent respectively in a radiation environment of 15 rad/h and 500 rad/h for LSO and LYSO samples of $2.5\times2.5\times20$ cm$^3$. Figure 9 (Left) shows an expanded view of the longitudinal transmittance spectra for three samples before and after several steps of the $\gamma$-ray irradiation with integrated dose of $10^2$, $10^4$ and $10^6$ rad. Also shown in the figure is the corresponding numerical values of the photo-luminescence weighted longitudinal transmittance ($EWLT$). Figure 9 (Right) shows the normalized average light output as a function of integrated dose for five long samples from various vendors. It is interesting to note that all samples show consistent radiation resistance with degradations of both the light output and transmittance at 10 to 15% level after $\gamma$-ray irradiation with an integrated dose of 1 Mrad.

Assuming the same APD based readout scheme as the CMS $PbWO_4$ calorimeter, the expected energy resolution of an LSO/LYSO crystal based electromagnetic calorimeter would be

$$\sigma_E/E = \mathbf{2}\%/\sqrt{E} \oplus \mathbf{0.5}\% \oplus 0.001/E, \quad (1)$$

which represents a fast calorimeter over large dynamic range with low noise. Such calorimeter would provide great physics discovery potential for high energy physics experiments in the proposed super B factory [12] as well as the proposed International Linear Collider (ILC) [13]. Because of its fast scintillation and good radiation hardness LYSO crystals are also proposed for the CMS $PbWO_4$ crystal endcap calorimeter upgrade at SLHC [14].

## 4. Crystal Hadronic Calorimeter

Crystals have recently been proposed to construct a homogeneous calorimeter, including both electromagnetic and hadronic part [3]. This homogeneous hadronic calorimeter concept removes the traditional boundary between ECAL and HCAL, so eliminates the effect of dead materials in the middle of the hadronic shower development. It takes advantage of recently implemented dual readout approach to measure both Cherenkov and scintillation light to achieve good energy resolution for hadronic jets measurement [4]. Because of the unprecedent volume (70 to 100 m$^3$) foreseen for such calorimeter [3], the crystal material must be dense (to reduce the volume),

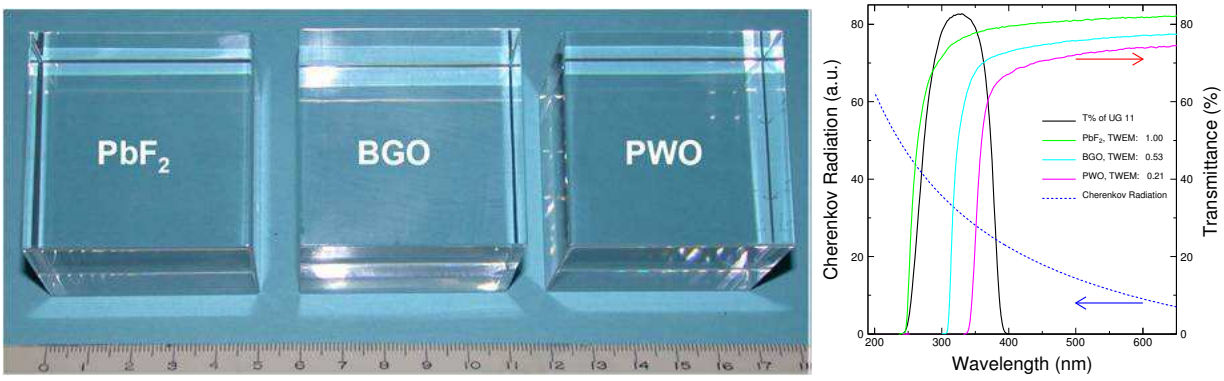


**Figure 10.** Left: A photo shows three crystal samples of $5\times5\times5$ cm$^3$ investigated for the homogeneous hadronic calorimeter concept. Right: The transmittance spectra of $PbF_2$ (green), BGO (blue), PWO (red) and UG11 (black) are shown as a function of wavelength. Also shown in this figure are the Cherenkov emission spectrum (dashed blue) and the normalized figure of merit for the Cherenkov light measurement with the UG11 filter.

UV transparent (to effective collecting the Cherenkov light) and allows a clear discrimination between the Cherenkov and scintillation light.

Figure 10 (Left) shows samples of three $5\times5\times5$ cm$^3$ crystal samples: $PbF_2$, BGO and PWO. Crystals of this size can be seen as typical building block for a crystal hadronic calorimeter. All material are dense ($PbF_2$ has of a density of 7.7 g/cm$^3$) with a nuclear interaction length about 22 cm. Mass production capability exists for all three candidate materials with cost among the lowest for materials of such density. Figure 10 (Right) shows the transmittance spectra of $PbF_2$ (green), BGO (blue), PWO (red) and a UG11 filter (black) as a function of wavelength together with the Cherenkov emission spectrum (dashed blue). The UG 11 filter can be used to select the Cherenkov light with small or no scintillation contamination. Also shown in this figure is the normalized figure of merit for the Cherenkov measurement (TWEM) by using the UG11 filter, which is defined as the transmittance weighted Cherenkov emission spectrum. Their numerical values are 1.0:0.53:0.21, which would be 1.0:0.82:0.75 without using the UG11 filter. Among these materials $PbF_2$ is the most effect in collecting the Cherenkov light because of its good UV transmission.

Effective discrimination between Cherenkov and scintillation light can be realized by using optical filter. Figure 11 (Left) shows a set-up used to investigate Cherenkov light collection and its separation from the scintillation light. Cosmic-rays were triggered by two finger counters with coincidence. The Cherenkov and scintillation light pulses generated by cosmic-rays were measured simultaneously by two Hamamatsu R2059 PMT coupled to the sample through optical filters UG11 and GG400. GG400 is a low-pass filter with cut-off at 400 nm. The UG11 filter is used to select the Cherenkov light as shown in Figure 10 (Right). The GG400 filter is used to select the scintillation light with small contamination of the Cherenkov light. The output of these two PMTs were digitized by an Agilent 6052A digital scope. Figure 11 (Middle and Right) shows the front edge of the scintillation light pulse from BGO and PWO, observed through the GG400 filter. Their delay from the trigger ($t_d$) and rise time ($t_r$) are identical with numerical values of 6.2 ns and 1.9 ns respectively. Figure 12 shows the Cherenkov light pulse shape observed for $PbF_2$ (Left), BGO (Middle) and PWO (Right) through the UG11 filter. All pulses have consistent time structure in the delay (6.1 ns), the rise time (1.8 ns), the fall time (4.2 ns) and the FWHM width (3.0 ns). It is interesting to note that there is no difference observed

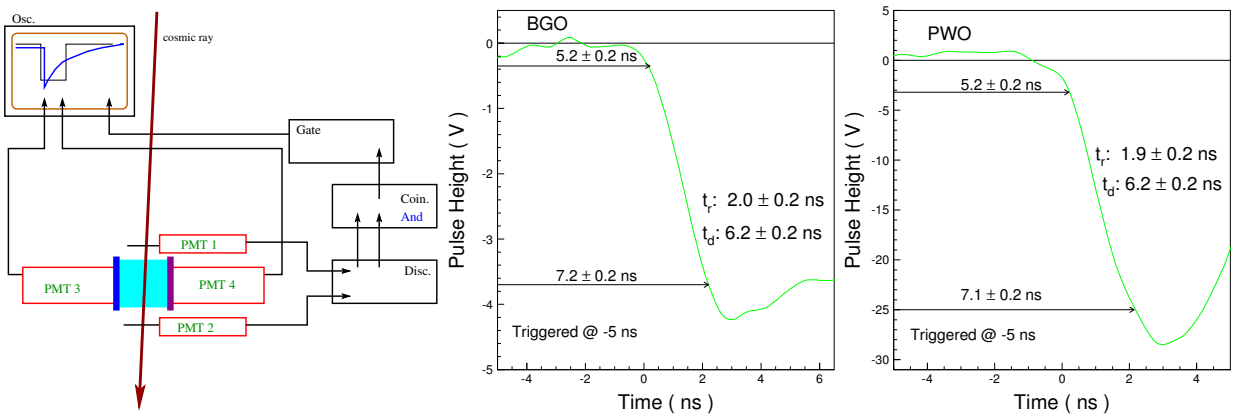


**Figure 11.** Left: A schematic showing a simple set-up used to measure cosmic-ray generated Cherenkov and scintillation light simultaneously by using two Hamamatsu R2059 PMT. The light pulses are recorded by an Agilent 6052A digital scope. Digital scope traces of the scintillation light front edge measured by a Hamamatsu R2059 PMT with GG400 filter for the BGO (Middle) and PWO (Right) samples.

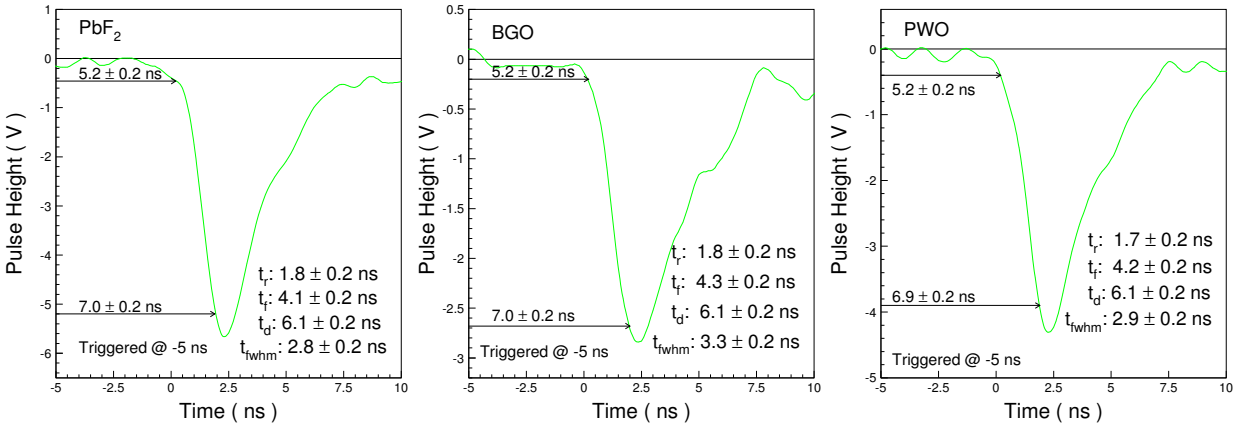


**Figure 12.** Digital scope traces of Cherenkov light pulse measured by a Hamamatsu R2059 PMT with UG11 filter for the $PbF_2$ (Left), BGO (Middle) and PWO (Right) samples.

in the delay and rise time between the Cherenkov and scintillation light, indicating that only the light pulse width and fall time are useful for the discrimination between the Cherenkov and scintillation light. A slow scintillator may help this discrimination.

The ratio of Cherenkov versus scintillation light was measured to be 1.55% and 22% for BGO and PWO respectively. These values are consistent with the scintillation light yield shown in Table 1, the emission weighed quantum efficiency of bi-alkali cathode of the Hamamatsu R2059 PMT shown in Figure 5 (Left) and the TWEM values shown in Figure 10 (Right).

Development of cost-effective material is crucial for the homogeneous hadronic calorimeter concept. While BGO is the best material to be used for such calorimeter, R&D is actively pursued by the high energy physics community for additional materials. One approach is to develop PWO crystals with slow scintillation emission . Green (560 nm) and slow emission with a few $\mu$sec decay time was observed by selective doping in PWO crystals [15]. Such crystals were reported to have a factor of ten more light than yttrium doped PWO crystals used in high energy physics experiment. This slow and green scintillation would be desirable for this application.

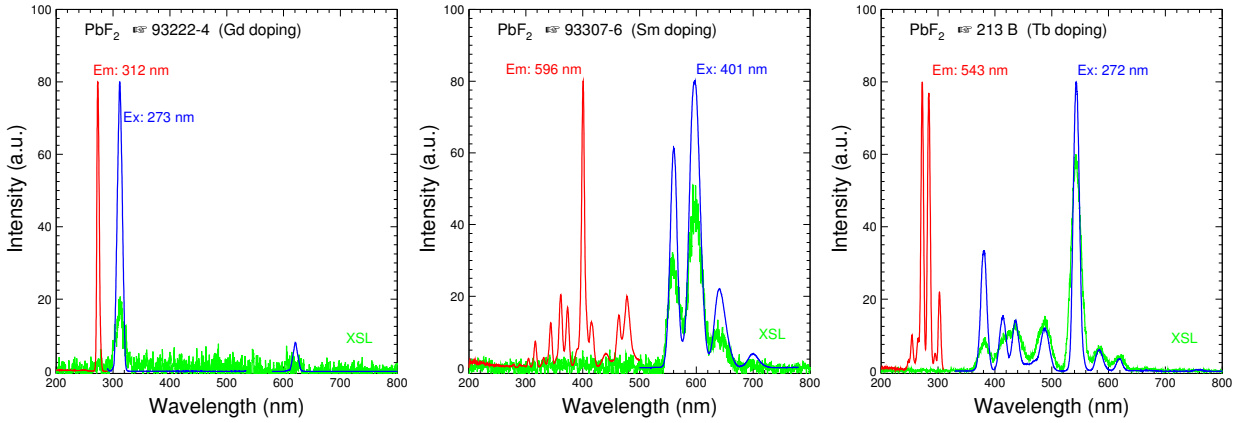


**Figure 13.** UV excitation (red), photo-luminescence (blue)and x-luminescence (green) spectra are shown as a function of wavelength for Gd (Left), Sm (Middle) and Tb (Right) dopes $PbF_2$ samples.

Another approach is to develop scintillating $PbF_2$ crystals by selective doping. Observations of fast scintillation in Gd or Eu doped $PbF_2$ crystals were reported [16, 17]. Our investigation shows that rear earth doping introduces scintillation in $PbF_2$, but not in the level can be measured by using $\gamma$-ray source. Figure 13 show the excitation, photo-luminescence and x-luminescence spectra for Gd, Sm and Tb doped $PbF_2$ crystal samples. It is noted that the scintillation of Sm and Tb doped $PbF_2$ samples is between 500 to 600 nm, which is desirable for Cherenkov/scintillation discrimination. Investigation is continuing aiming at developing cost-effective materials for this concept.

## 5. Summary

Precision crystal electromegnetic calorimeters have been an important part of high energy physics detector. In addition to the Panda PWO electromagnetic calorimeter at Fair [18] the availability of mass production capability of large size LSO and LYSO crystals provides an opportunity to build a LSO/LYSO crystal electromegnetic calorimeter with unprecedent energy resolution over a large dynamic range down to MeV level. Such calorimeter, if built, would greatly enhance the physics discovery potential for high energy and nuclear physics experiments in the next decade.

Recent interest in high energy physics community to pursue homogeneous hadronic calorimeter with dual readout opens a new area of crystal calorimetry to achieve good energy resolution for hadronic jets in the next decade. The main challenge for this concept is to develop cost effective heavy crystal scintillators with good UV transmission and excellent Cherenkov/scintillation discrimination.

## Acknowledgments

This work is partially supported by the U.S. Department of Energy Grant No. DE-FG03-92-ER40701 and the U.S. National Science Foundation Award PHY-0612805 and PHY-0516857.

## References

[1] G. Gratta, H. Newman and R.-Y. Zhu, *Annu. Rev. Nucl. Part. Sci.* **44** 453 (1994).
[2] R.-Y. Zhu, in *Proceedings of XII International Conference on Calorimetry in Particle Physics*, Ed. S. Magill and R. Yoshida, AIP Conference Proceedings Volume 867 (2006) 64.
[3] A. Para, http://ilcagenda.linearcollider.org/contributionDisplay.py?contribId=15&sessionId=3&confId=2474.
[4] R. Wigmans, in *Proceedings of VII International Conference on Calorimetry in Particle Physics*, Ed. E. Chen *et al.*, World Scientific (1998) 182, and N. Akchurin *et al.*, *Nucl. Instr. and Meth.* **A537** (2005) 537. Also, see papers in these Proceedings.
[5] C. Melcher, V.S. Patent 4958080 (1990) and 5025151 (1991).
[6] D.W. Cooke, K.J. McClellan, B.L. Bennett, J.M. Roper, M.T. Whittaker and R.E. Muenchausen, *J. Appl. Phys.* **88** (2000) 7360 and T. Kimble, M Chou and B.H.T. Chai, *2002 IEEE NSS Conference Record.*
[7] E. Loef, P. Dorenbos, E. Eijk, K. Kraemer and H. Guedel, *Nucl. Instr. and Meth.* **A486** (2002) 254.
[8] R.H. Mao, L.Y. Zhang and R.-Y. Zhu, *IEEE Trans. Nucl. Sci.* **NS-55** (2008).
[9] D.A. Ma and R.-Y. Zhu, *Nucl. Instr. and Meth.* **A333** (1993) 422.
[10] J.M. Chen, R.H. Mao, L.Y. Zhang and R.-Y. Zhu, *IEEE Trans. Nucl. Sci.* **54** (2007) 718.
[11] J.M. Chen, R.H. Mao, L.Y. Zhang and R.-Y. Zhu, *IEEE Trans. Nucl. Sci.* **54** (2007) 1319.
[12] SuperB Conceptual Design Report, **INFN/AE-07/2, SLAC-R-856, LAL 07-15**, March (2007).
[13] R.-Y. Zhu, *A LSO/LYSO Crystal Calorimeter for the ILC*, talk presented in 2005 ILC Workshop, Snowmass. http://nicadd.niu.edu/cdsagenda//fullAgenda.php?ida=a0561.
[14] R.-Y. Zhu, *Development of LYSO Crystals for CMS at SLHC*, talk presented in CMS ECAL SLHC Workshop, CERN. http://www.hep.caltech.edu/ zhu/talks/ryz_080415_SLHC.pdf.
[15] R.H. Mao *et al.*, in *Proceedings of IX International Conference on Calorimetry in Particle Physics*, Ed. B. Aubert *et al.*, Franscati Physics Series Vol. XXI (2000) 709-720.
[16] D. Shen *et al.*, *Jour. Inor. Mater.* **Vol 101** (1995) 11.
[17] C. Woody *et al.*, in *Proceedings of SCINT95*, Delft University Press, Delft, The Netherlands, (1996).
[18] Philippe Rosier, in these Proceedings.